https://ntrs.nasa.gov/search.jsp?R=19930086821 2020-06-17T14:06:56+00:00Z

FILE COPY
NO 2

NACA RM L51H09a

NACA

RESEARCH MEMORANDUM

EXPERIMENTAL AND ANALYTICAL INVESTIGATION OF FLUTTER OF A NONUNIFORM SWEPTBACK CANTILEVER WING WITH TWO CONCENTRATED WEIGHTS

By John L. Sewall

Langley Aeronautical Laboratory
Langley Field, Va.

DOCUMENT ON LOAN FROM THE FILES OF
NATIONAL ADVISORY COMMITTEE FOR AERONAUTICS
LANGLEY AERONAUTICAL LABORATORY
LANGLEY FIELD, HAMPTON, VIRGINIA
RETURN TO THE ABOVE ADDRESS
REQUESTS FOR PUBLICATIONS SHOULD BE ADDRESSED AS FOLLOWS:
NATIONAL ADVISORY COMMITTEE FOR AERONAUTICS
1512 H STREET, N. W.
WASHINGTON 25, D. C.

NATIONAL ADVISORY COMMITTEE
FOR AERONAUTICS

WASHINGTON

December 4, 1951

NATIONAL ADVISORY COMMITTEE FOR AERONAUTICS

RESEARCH MEMORANDUM

EXPERIMENTAL AND ANALYTICAL INVESTIGATION OF FLUTTER OF A NONUNIFORM SWEPTBACK CANTILEVER WING WITH TWO CONCENTRATED WEIGHTS

By John L. Sewall

SUMMARY

The results of an experimental and analytical investigation of the flutter characteristics of a nonuniform sweptback cantilever wing are presented. The angle of sweep was 34.5° and concentrated weights which were 78.4 percent and 42.0 percent of the weight of the wing were mounted at approximately one-third and three-quarters of the span, respectively. The experimental information was obtained in the Langley 4.5-foot flutter research tunnel, and a Rayleigh-Ritz type of analysis was employed in the flutter calculations.

Correlation of experiment with theory based on uncoupled still-air vibration modes is demonstrated for this swept-wing configuration. The flutter calculations using just two modes gave results which were only 7 percent conservative, and this agreement is considered good in view of the fact that two eccentrically mounted concentrated weights were included in the configuration. The use of three and four uncoupled modes in the analysis produced only a small change in the results obtained with two uncoupled modes. This fact implies that the analytical results with two modes had closely converged on an answer which for practical purposes is the limit of convergence of the Rayleigh-Ritz process for this case.

For completeness, related theoretical information is included in an appendix, and this information consists of the determinantal flutter equation and general expressions for the determinant elements for any number of uncoupled modes.

INTRODUCTION

Experimental and analytical studies of flutter of a uniform unswept cantilever wing carrying a variably located concentrated weight are reported in references 1 to 4. Reference 1 provides an experimental

background which consists of the results of flutter tests made with a single concentrated weight mounted at various spanwise and chordwise positions on the wing. Some of these results are analyzed in reference 2 by the direct solution of the differential equations of motion of the wing during flutter. This type of analysis yields a solution which is exact within the bounds of simple beam theory but this type of analysis is impracticable for application to an actual airplane wing. In references 3 and 4 a Rayleigh-Ritz type of flutter analysis is applied to selected cases from reference 1 to investigate the validity of certain modal approximations involved in the analysis. These investigations were made with the use of uncoupled modes in reference 3 and coupled modes in reference 4. For each flutter calculation these modes were based on the elastic and inertial properties of the wing-weight system under consideration.

The flutter of swept wings without concentrated weights is studied in reference 5, in which the oscillating two-dimensional aerodynamic forces and moments of reference 6 have been modified to account for the effects of sweep. Uniform cantilever wings having sweep angles up to 60° were analyzed by means of a Rayleigh-Ritz approach in reference 5; the modal functions used were uncoupled first bending and first torsion modes for an ideal uniform cantilever beam.

The present paper is a continuation of the work presented in the references mentioned in the foregoing discussion and has as its objective the correlation of theory with experiment for a nonuniform sweptback cantilever wing carrying concentrated weights at two widely separated positions along the length of the wing. The aerodynamic forces and moments derived in reference 5 are used. The uncoupled modes included in the analysis were determined from the measured elastic and inertial properties of the wing-weight configuration. As many as four such modes were used in the analysis. Experimental flutter data were obtained with both concentrated weights mounted on the wing for two different root conditions. In one of these conditions the root section was clamped parallel to the air stream in the usual manner for sweptback wings. In the other condition a triangular-shaped area at the root was restrained so that the wing behaved structurally as an unswept cantilever beam.

Additional information of a related nature is presented in an appendix. This information is concerned with the theoretical aspects of the problem and contains the determinantal flutter equation together with expressions for the determinant elements for any number of uncoupled modes.

SYMBOLS

a	nondimensional distance of elastic axis relative to midchord, from midchord measured perpendicular to elastic axis
b	half-chord of wing measured perpendicular to elastic axis, feet
b_r	half-chord of wing measured perpendicular to elastic axis at reference station, feet
c	chord in air-stream direction, feet
EI	bending stiffness of wing, pound-feet^2
f_e	experimental flutter frequency, cycles per second
f_i	experimental natural frequency in ith coupled mode, cycles per second
f_Λ	theoretical flutter frequency, cycles per second
$F_{h_i}(\eta)$	amplitude function of wing in ith bending mode
$F_{\theta_i}(\eta)$	amplitude function of wing in ith torsion mode
GJ	torsional stiffness of wing, pound-feet^2
g_i	structural-damping coefficient in ith coupled mode
h	bending deflection of elastic axis, positive downward, feet
I_α	mass moment of inertia of wing per unit length about elastic axis, slug-feet
k_n	reduced frequency referred to velocity component perpendicular to elastic axis $(\omega b/v_n)$
l'	length of wing measured along elastic axis, feet
m	mass of wing per unit length along elastic axis, slugs per foot
M	Mach number

r_α nondimensional radius of gyration of wing about elastic axis $\left(\sqrt{\frac{I_\alpha}{mb^2}}\right)$

t time, seconds

v free-stream velocity, feet per second

v_e experimental flutter speed in air-stream direction, feet per second

v_i experimental indicated flutter speed in air-stream direction, feet per second $\left(v_e\sqrt{\frac{\rho}{\rho_o}}\right.$ where ρ_o is density of air under standard conditions in slugs per cubic foot$\left.\right)$

v_n component of air-stream velocity perpendicular to elastic axis, feet per second $(v \cos \Lambda)$

v_Λ theoretical flutter velocity in air-stream direction, feet per second

x_α nondimensional location of center of gravity, relative to midchord, from elastic axis measured perpendicular to elastic axis

y' coordinate along elastic axis, feet

η nondimensional coordinate along elastic axis (y'/l')

θ torsional deflection of elastic axis, positive with leading edge up, radians

κ mass-density ratio at flutter $(\pi\rho b^2/m)$

Λ angle of sweep, degrees

ρ density of testing medium, slugs per cubic foot

ω angular frequency of vibration, radians per second

ω_{h_i} angular frequency of ith uncoupled bending mode, radians per second

ω_{α_i} angular frequency of ith uncoupled torsion mode, radians per second

EXPERIMENTAL APPARATUS AND TEST PROCEDURE

Wing.- The model tested in this program was a nonuniform cantilever wing with the 38-percent-chord line swept back 34.5° as shown in figure 1 and built of laminated balsa wood with a dural insert. In figure 2 the detailed cross-sectional views at the root and tip show this type of construction more clearly.

In order that the structural properties of the wing nearly fulfill the requirements of the analytical assumption of a straight elastic axis, these quantities were measured with a rigid restraint of bismuth and tin alloy molded to the root. The manner in which this restraint was mounted can be seen in the general view of the wing in the test section (fig. 3). The restraint was made perpendicular to a line located at 38 percent of the chord (in the air-stream direction). Figure 1 indicates the location of the measured centers of gravity and also the measured elastic centers which determine the location of the elastic axis. The corresponding values of x_{α} and a are given in table I.

The lengthwise variations in bending and torsional stiffness are given in figure 4. The definite increase in torsional stiffness near each of the concentrated weight positions is attributed to the attachment of the weight mounts in a plane skewed relative to the plane in which static loads were applied to measure stiffness.

The lengthwise distributions of mass and mass moment of inertia (see figs. 5 and 6, respectively) were obtained (after the flutter runs were completed) by cutting the wing into twelve segments perpendicular to the 38-percent-chord line (segment numbers indicated along trailing edge of wing in fig. 1). Figure 7 presents the lengthwise variation in mass-density ratio (shown as $1/\kappa$) for each flutter run. In run 1 the root restraint was mounted on the wing and in run 2 the root restraint was removed. Values for the square of the radius of gyration are given in table I. Other properties of the wing are as follows:

Geometric aspect ratio (based on the half-wing)	4.64
Taper ratio (tip chord to root chord in air-stream direction)	0.428
Airfoil section, parallel to air stream	NACA 65_1-012
Weight of wing, pounds	3.79

Concentrated weights.- Two concentrated weights, made from an alloy of bismuth and tin, were located on the wing at approximately one-third and three-quarters of the span as shown in figure 1. The inboard weight was 78.4 percent and the outboard weight was 42.0 percent of the weight of the wing. Both weights were rigidly attached to $\frac{1}{8}$-inch-thick dural

weight mounts which in turn were rigidly fastened to the dural insert of the wing in the air-stream direction. The positions of the weights on the weight mounts remained unchanged during the test program.

Testing equipment and procedure.- The experimental program was conducted in the Langley 4.5-foot flutter research tunnel at nearly atmospheric pressure in a mixture of air and Freon-12 in the ratio of approximately 1 to 9. Bending and torsional strains of the wing during flutter were recorded electrically by the use of resistance-wire strain gages mounted at the locations indicated in figure 1. The strain-gage signals were fed through a system of electrical bridges and amplifiers into a recording oscillograph. Portions of the oscillograph records at flutter for both runs are shown in figure 8. The flutter frequencies were obtained from these records. These frequencies along with other pertinent data are given in table II. The structural-damping coefficients were determined from the rate of decay of oscillations in still air on the vibration records of the natural frequencies.

The wing was excited in its natural frequencies before and after each run to determine whether the internal structure of the wing had been damaged by flutter. Also during flutter the wing was photographed by means of a high-speed motion-picture camera located outside the tunnel in the position indicated in figure 9. Figure 10 shows two sequences of pictures taken with this camera. The flutter oscillations for run 2 (without root restraint) can be seen in figure 10(a), whereas those of a similar model, which fluttered to destruction, appear in figure 10(b).

Experimental results.- Comparison of the flutter data for both runs in table II shows that the indicated flutter speed of the wing-weight configuration with the root restraint installed was approximately $2\frac{1}{2}$ percent higher than that without root restraint. The flutter frequency was increased by approximately 12 percent with the addition of the root restraint.

The effect of the root restraint on the natural modes of vibration may be seen by examining the natural frequencies given in table II. In order to identify the natural frequencies in table II according to their bending and torsional characteristics, further experimental study of the natural modes of vibration was conducted for the same wing-weight configuration having a wing built to the same specifications as the subject wing. The results of this study are given in figure 11 which shows the nodal patterns and corresponding natural frequencies for the first three modes of vibration. The root condition shown in figure 11(a) is similar to that for run 1 in table II and the root condition in figure 11(b) is similar to that for run 2 in table II. The first mode, designated by f_{h_1} in figure 11, is predominantly first bending; the second mode,

designated by f_{h_2}, is predominantly second bending; and the third mode, designated by f_{t_1}, is predominantly first torsion. Comparison of the frequency data in this figure with the corresponding frequency data in table II shows that the natural frequencies f_1, f_2, and f_3 may be described as first bending, second bending, and first torsion, respectively. It may be of interest to point out that a comparison of the ratio of first bending to first torsion f_1/f_3 for run 1 with that for run 2 shows an increase of about 7.3 percent due to the root restraint condition and that this increase is of the same order of magnitude as the corresponding increase in flutter frequency.

ANALYTICAL INVESTIGATION

Method of analysis.- As pointed out in the introduction, this paper employs a Rayleigh-Ritz type of flutter analysis in which the flutter mode is approximated by a combination of chosen modal functions. Many such functions could be used but the ones usually selected are either the coupled or uncoupled modes of vibration of the system. The present paper made use of uncoupled modes which were determined by calculations based on the measured elastic and inertial properties of the system.

With the use of generalized coordinates, each mode is assumed to represent a degree of freedom. For each degree of freedom the section properties are integrated over the length of the wing to obtain the kinetic and potential energies together with the work done on the wing by the structural and aerodynamic forces. In the aerodynamic part of the problem the effect of sweep is taken into account by the method developed in reference 5. In the structural part of the problem the root section is assumed to be sufficiently stiff so that the wing behaves as if it were clamped normal to the elastic axis, and the elastic axis is assumed to lie entirely within the boundaries of the main part of the wing. Experimental data gathered with the use of a root restraint indicate that these assumptions are fairly well justified for conventional swept wings of moderate length-chord ratio.

Once the integrated expressions involving the energies and work done by structural and aerodynamic forces are determined, the equation of equilibrium, given by Lagrange's equation, may be written for each degree of freedom. Each equation then becomes one of a set of simultaneous homogeneous equations, and the condition of consistency of these equations leads to the flutter condition. This procedure is discussed further in appendix A, not only for three degrees of freedom but also for any number of freedoms. General expressions are also given in this appendix for the coefficients in the equilibrium equations for any number of degrees of freedoms.

Application of method of analysis.- In the application of this type of analysis to the general case of a weighted nonuniform sweptback wing, the lengthwise variation in structural and aerodynamic properties must be taken into consideration in accordance with the foregoing assumptions regarding the angle of sweep. In the present paper the distribution of elastic and inertial properties over the main part of the wing were determined for an arbitrary number of lengthwise segments taken perpendicular to the elastic axis. In determining the aerodynamic forces use was made of reference 7 in which the aerodynamic functions derived in reference 6 appear in useful form for flutter calculations. In order to take into account, partially, the effects of wing taper on these quantities, the variation in the reduced wave length $1/k_n$ over the length of the wing was considered, and the aerodynamic functions corresponding to each $1/k_n$ were determined with the aid of reference 8 in which the tabulated lift and moment data from reference 7 are fitted to families of overlapping parabolas.

As previously mentioned, uncoupled modes were employed for the wing-weight system analyzed in this paper. These modes, based on the elastic and inertial properties of the present configuration, were calculated using the iterative procedure of reference 9 and are presented in figure 12 along with their corresponding frequencies. The slopes of the first and second bending modes are given in figure 13.

With the elastic, inertial, and aerodynamic properties known for each section along the length of the wing, the integrated expressions for the coefficients in the equilibrium equations were computed and the determinant of these coefficients was solved to obtain the flutter condition. The determinants involving three and four degrees of freedom were solved by the iterative method presented in reference 10. This method is particularly well-adapted to The Bell Telephone Laboratories X-66744 relay computer at the Langley Laboratory which was used in performing these calculations.

ANALYTICAL RESULTS AND CORRELATION OF THEORY AND EXPERIMENT

In table III the results of flutter calculations are compared with experimental results for the subject sweptback wing with two concentrated weights. Pursuant to the foregoing analytical assumptions all calculations were based on the structural properties and parameters corresponding to the restrained root condition. Hence, the differences between the analytical results for restrained and unrestrained root conditions (runs 1 and 2, respectively) are due to the difference in density between the two conditions. For investigating the effects of

introducing higher uncoupled modes into the analysis, the tunnel conditions corresponding to run 1 were used. The structural-damping coefficients were assumed to be zero in all calculations. The tabulated theoretical flutter speeds and flutter frequencies were obtained from conventional plots of these quantities against the theoretical damping coefficient. The characteristics of these curves were such that no significant change would have been encountered had structural damping been included.

In discussing these results particular attention is directed toward the flutter speed. As can be seen in table III the theoretical flutter speed was approximately 7 percent conservative when just two modes, first bending and first torsion, were employed in the analysis. This agreement is considered remarkably good in view of the fact that two eccentrically mounted concentrated weights were located on the wing. Judging from the results of reference 3, one would suspect that higher uncoupled modes should have been included in the analysis to obtain a theoretical flutter speed as satisfactory as that obtained using just two modes. However, in this instance the theoretical flutter speed was not significantly altered when various combinations of second bending and second torsion modes were added. This fact indicates that, with the use of the first bending and first torsion modes of the present wing-weight system, the Rayleigh-Ritz process, as applied to this configuration, had satisfactorily converged on an answer which for practical purposes is the same as would have been obtained with any number of higher-order modes added.

The results also show that the oscillating aerodynamic forces and moments, based on two-dimensional incompressible flow as modified in reference 5 to account for the effect of sweep, were adequate for this configuration.

CONCLUDING REMARKS

Flutter data are reported for a nonuniform sweptback cantilever wing carrying two eccentrically mounted concentrated weights. The wing was fluttered with and without a restraint molded to the triangular area at the root. The results of these experiments provide further evidence justifying the commonly employed assumptions of a nonskewed root section and a straight elastic axis over the main part of the wing in the flutter analyses of swept wings of moderate length-chord ratios.

A Rayleigh-Ritz type of flutter analysis, employing uncoupled modal functions, was applied to this wing-weight system with the use of the properties appropriate to the restrained root condition. The calculated flutter speeds based on two modes (first bending and first

torsion) were about 7 percent conservative. The fact that this agreement with experiment was not appreciably altered when higher modes (namely, second bending and second torsion) were added indicates that in the present application of this process the theoretical limit of convergence had, for practical purposes, been obtained with only two modes. Furthermore, the small difference between theory and experiment shows that the use of the two modes gave satisfactory results.

The theoretical oscillating aerodynamic forces and moments for two-dimensional flow, as modified for sweep, were found to be adequate for the configuration studied.

Langley Aeronautical Laboratory
National Advisory Committee for Aeronautics
Langley Field, Va.

APPENDIX A

OUTLINE OF SWEPT-WING FLUTTER ANALYSIS EMPLOYING ANY NUMBER OF UNCOUPLED MODES

The manner in which higher-order modal functions are introduced into the Rayleigh-Ritz type of flutter analysis described in the body of this paper is demonstrated herein. The swept-wing analysis in reference 5 was developed in detail for two modes: first bending and first torsion. Integrated expressions involving the total energy and work done by applied forces for more than two modes may be readily obtained by following the procedure of reference 5. Consider, for example, the inclusion of a second bending mode. Then the mode shapes may be represented by the following equations:

For first bending

$$h_1 = \left[F_{h_1}(\eta)\right] \underline{h}_1 \tag{A1a}$$

For second bending

$$h_2 = \left[F_{h_2}(\eta)\right] \underline{h}_2 \tag{A1b}$$

For first torsion

$$\theta_1 = \left[F_{\theta_1}(\eta)\right] \underline{\theta}_1 \tag{A1c}$$

where $\left[F_{h_1}(\eta)\right]$, $\left[F_{h_2}(\eta)\right]$, and $\left[F_{\theta_1}(\eta)\right]$ are amplitude functions which may in general be complex but in the present application are chosen as real quantities. The quantities $\underline{h}_1$, $\underline{h}_2$, and $\underline{\theta}_1$ are generalized coordinates in the three degrees of freedom defined as follows:

$$\underline{h}_1 = h_{o_1} e^{i\omega t}$$

$$\underline{h}_2 = h_{o_2} e^{i\omega t}$$

$$\underline{\theta}_1 = \theta_{o_1} e^{i\omega t}$$

where h_{o_1}, h_{o_2}, and θ_{o_1} are, in general, complex quantities signifying phase differences among the degrees of freedom.

The general equation of equilibrium for each degree of freedom, using Lagrange's equation, is

$$\frac{d}{dt}\left(\frac{\partial T}{\partial \dot{q}_m}\right) - \frac{\partial T}{\partial q_m} + \frac{\partial U}{\partial q_m} = Q_m \tag{A2}$$

where T and U represent, respectively, the total kinetic and potential energies of the system, Q_m represents the generalized aerodynamic and structural-damping forces appropriate to the mth degree of freedom, and q_m is the generalized coordinate. With the application of equation (A2), the generalized coordinate q_m in each of the three equations becomes successively $\underline{h}_1$, $\underline{h}_2$, and $\underline{\theta}_1$ and the corresponding aerodynamic and structural-damping forces are represented by Q_{h_1}, Q_{h_2}, and Q_{θ_1}, respectively. The introduction of these quantities into equation (A2) and the performance of some algebraic manipulations leads to the equations of equilibrium in the following form:

$$\left(\frac{\underline{h}_1}{b_r}A_{11} + \frac{\underline{h}_2}{b_r}A_{12} + \underline{\theta}_1 B_{11}\right)\pi\rho b_r^3\omega^2 l' = 0 \tag{A3}$$

$$\left(\frac{\underline{h}_1}{b_r}A_{21} + \frac{\underline{h}_2}{b_r}A_{22} + \underline{\theta}_1 B_{21}\right)\pi\rho b_r^3\omega^2 l' = 0 \tag{A4}$$

$$\left(\frac{\underline{h}_1}{b_r}D_{11} + \frac{\underline{h}_2}{b_r}D_{12} + \underline{\theta}_1 E_{11}\right)\pi\rho b_r^4\omega^2 l' = 0 \tag{A5}$$

Note that these equations form a homogeneous system of equations in $\frac{\underline{h}_1}{b_r}$, $\frac{\underline{h}_2}{b_r}$, and $\underline{\theta}_1$; thus, the necessary condition that the system has solutions, other than the trivial solution, is that the determinant of the coefficients vanishes, namely:

$$\begin{vmatrix} A_{11} & A_{12} & B_{11} \\ A_{21} & A_{22} & B_{21} \\ D_{11} & D_{12} & E_{11} \end{vmatrix} = 0 \tag{A6}$$

This equation can be shown to correspond to a borderline condition separating damped from undamped oscillations, which is the flutter condition.

The foregoing procedure may be extended to include many such freedoms, both bending and torsion. The determinantal equation (or

flutter determinant) for the general case may be written as follows:

$$\begin{vmatrix} A_{ij} & B_{ij} \\ D_{ij} & E_{ij} \end{vmatrix} = 0 \tag{A7}$$

in which the elements "A" contain solely bending terms, the elements "B" and "D" contain cross-coupling terms between bending and torsion, and the elements "E" contain solely torsion terms; the elements "A" and "E" containing the unknown flutter frequency appear in the principal diagonal and are denoted by two identical subscripts. The following expressions for these elements are written for R uncoupled bending modes and S uncoupled torsion modes, as subsequently indicated by subscripts.

The terms enclosed by the brackets $\langle\ \rangle$ account for effects associated with the first derivative of torsion with respect to span direction, the second derivative of bending with respect to span direction, and the second derivative of torsion with respect to span direction. These terms were not included in the present calculations, since limited experience has shown a relatively small contribution from these terms even for large angles of sweep on uniform wings (see reference 5). However, in flutter analyses on highly swept wings carrying concentrated weights, these bracketed terms may prove significant.

The flutter determinant elements are

$$A_{ij} = -\int_0^{1.0}\left(\frac{b}{b_r}\right)^2 A_{ch}\left[F_{h_i}(\eta)\right]\left[F_{h_j}(\eta)\right]d\eta + \frac{b_r}{l'}\int_0^{1.0}\left(\frac{b}{b_r}\right)^3 \tan\Lambda\left(i\frac{1}{k_n}\right)\left(\left\langle -1\right\rangle + A_{ch}\right)\left[F_{h_i}(\eta)\right]\frac{d}{d\eta}\left[F_{h_j}(\eta)\right]d\eta - \left\langle\left(\frac{b_r}{l'}\right)^2\int_0^{1.0}\left(\frac{b}{b_r}\right)^4\tan^2\Lambda\left(\frac{1}{k_n}\right)^2\left[F_{h_i}(\eta)\right]\frac{d^2}{d\eta^2}\left[F_{h_j}(\eta)\right]d\eta\right\rangle \qquad (i \neq j) \tag{A8}$$

where

$$i = 1, 2, 3, \ldots R$$

$$j = 1, 2, 3, \ldots R$$

$$A_{ii} = \left[1 - \left(\frac{\omega_{h_i}}{\omega}\right)^2\left(1 + ig_{h_i}\right)\right]\int_0^{1.0}\left(\frac{b}{b_r}\right)^2 \frac{1}{\kappa}\left[F_{h_i}(\eta)\right]^2 d\eta -$$

$$\int_0^{1.0}\left(\frac{b}{b_r}\right)^2 A_{ch}\left[F_{h_i}(\eta)\right]^2 d\eta +$$

$$\frac{b_r}{l'}\int_0^{1.0}\left(\frac{b}{b_r}\right)^3 \tan\Lambda\left(i\frac{1}{k_n}\right)\left(\langle -1\rangle + A_{ch}\right)\left[F_{h_i}(\eta)\right]\frac{d}{d\eta}\left[F_{h_i}(\eta)\right] d\eta -$$

$$\left\langle\left(\frac{b_r}{l'}\right)^2\int_0^{1.0}\left(\frac{b}{b_r}\right)^4 \tan^2\Lambda\left(\frac{1}{k_n}\right)^2\left[F_{h_i}(\eta)\right]\frac{d^2}{d\eta^2}\left[F_{h_i}(\eta)\right] d\eta\right\rangle \qquad (A9)$$

for the principal diagonal element in bending, in which $i = j$ and g_{h_i} is the coefficient of structural damping in the ith bending mode,

$$B_{ij} = \int_0^{1.0}\left(\frac{b}{b_r}\right)^3\left(\frac{x_\alpha}{\kappa} - A_{c\alpha}\right)\left[F_{h_i}(\eta)\right]\left[F_{\theta_j}(\eta)\right] d\eta -$$

$$\left\langle\frac{b_r}{(l')^2}\int_0^{1.0}\left(\frac{b}{b_r}\right)^4 \tan\Lambda\left(A_{c\tau}\right)\left[F_{h_i}(\eta)\right]\frac{d}{d\eta}\left[F_{\theta_j}(\eta)\right] d\eta -\right.$$

$$\left.\left(\frac{b_r}{l'}\right)^2\int_0^{1.0}\left(\frac{b}{b_r}\right)^5 \tan^2\Lambda\left(\frac{a}{k_n^2}\right)\left[F_{h_i}(\eta)\right]\frac{d^2}{d\eta^2}\left[F_{\theta_j}(\eta)\right] d\eta\right\rangle \qquad (A10)$$

where

$$i = 1, 2, 3, \ldots R$$

$$j = 1, 2, 3, \ldots S$$

$$D_{ij} = \int_0^{1.0}\left(\frac{b}{b_r}\right)^3\left(\frac{x_\alpha}{\kappa} - A_{ah}\right)\left[F_{\theta_i}(\eta)\right]\left[F_{h_j}(\eta)\right] d\eta +$$

$$\frac{b_r}{l'}\int_0^{1.0}\left(\frac{b}{b_r}\right)^4 \tan\Lambda\left(i\frac{1}{k_n}\right)\left(\langle a\rangle + A_{ah}\right)\left[F_{\theta_i}(\eta)\right]\frac{d}{d\eta}\left[F_{h_j}(\eta)\right] d\eta +$$

$$\left\langle\left(\frac{b_r}{l'}\right)^2\int_0^{1.0}\left(\frac{b}{b_r}\right)^5 \tan^2\Lambda\left(\frac{a}{k_n^2}\right)\left[F_{\theta_i}(\eta)\right]\frac{d^2}{d\eta^2}\left[F_{h_j}(\eta)\right] d\eta\right\rangle \qquad (A11)$$

where

$$i = 1, 2, 3, \ldots S$$

$$j = 1, 2, 3, \ldots R$$

$$E_{ij} = -\int_0^{1.0}\left(\frac{b}{b_r}\right)^4 A_{a\alpha}\left[F_{\theta_i}(\eta)\right]\left[F_{\theta_j}(\eta)\right]d\eta -$$

$$\left\langle \frac{b_r}{l'}\int_0^{1.0}\left(\frac{b}{b_r}\right)^5 \tan\Lambda\left(A_{a\tau}\right)\left[F_{\theta_i}(\eta)\right]\frac{d}{d\eta}\left[F_{\theta_j}(\eta)\right]d\eta + \right.$$

$$\left.\left(\frac{b_r}{l'}\right)^2\int_0^{1.0}\left(\frac{b}{b_r}\right)^6 \tan^2\Lambda\left(\frac{1}{8}+a^2\right)\left(\frac{1}{k_n}\right)^2\left[F_{\theta_i}(\eta)\right]\frac{d^2}{d\eta^2}\left[F_{\theta_j}(\eta)\right]d\eta\right\rangle$$

$$(i \neq j) \qquad (A12)$$

where

$$i = 1, 2, 3, \ldots S$$

$$j = 1, 2, 3, \ldots S$$

$$E_{ii} = \left[1 - \left(\frac{\omega_{\alpha_i}}{\omega}\right)^2\left(1 + ig_{\alpha_i}\right)\right]\int_0^{1.0}\left(\frac{b}{b_r}\right)^4 \frac{r_\alpha^2}{\kappa}\left[F_{\theta_i}(\eta)\right]^2 d\eta -$$

$$\int_0^{1.0}\left(\frac{b}{b_r}\right)^4 A_{a\alpha}\left[F_{\theta_i}(\eta)\right]^2 d\eta -$$

$$\left\langle \frac{b_r}{l'}\int_0^{1.0}\left(\frac{b}{b_r}\right)^5 \tan\Lambda(A_{a\tau})\left[F_{\theta_i}(\eta)\right]\frac{d}{d\eta}\left[F_{\theta_i}(\eta)\right]d\eta + \right.$$

$$\left.\left(\frac{b_r}{l'}\right)^2\int_0^{1.0}\left(\frac{b}{b_r}\right)^6 \tan^2\Lambda\left(\frac{1}{8}+a^2\right)\left(\frac{1}{k_n}\right)^2\left[F_{\theta_i}(\eta)\right]\frac{d^2}{d\eta^2}\left[F_{\theta_i}(\eta)\right]d\eta\right\rangle \qquad (A13)$$

for the diagonal element in torsion, in which $i = j$ and $g_{\alpha i}$ is the coefficient of structural damping in the ith torsion mode.

The quantities A_{ch}, $A_{c\alpha}$, A_{ah}, $A_{a\alpha}$, $A_{c\tau}$, and $A_{a\tau}$ represent expressions for oscillating lift and moment as defined in reference 5 in terms of the functions derived in reference 6. Equivalent forms of these expressions in terms of L_h, L_α, M_h, and M_α from reference 7 are as follows:

$$A_{ch} = - L_h$$

$$A_{c\alpha} = - L_\alpha + \left(\frac{1}{2} + a\right) L_h$$

$$A_{ah} = - M_h + \left(\frac{1}{2} + a\right) L_h$$

$$A_{a\alpha} = - M_\alpha + \left(\frac{1}{2} + a\right)(L_\alpha + M_h) - \left(\frac{1}{2} + a\right)^2 L_h$$

$$A_{c\tau} = \left(\frac{1}{k_n}\right)^2 - i\frac{1}{k_n}\left[M_h(1 - L_h) + a(1 + L_h)\right]$$

$$A_{a\tau} = - \left(\frac{1}{k_n}\right)^2 - \frac{1}{k_n}\left(\frac{1}{2} + a\right) + i\frac{1}{k_n}\left[M_\alpha + \left(\frac{1}{8} + a^2\right) - \left(\frac{1}{4} - a^2\right)L_h\right]$$

where

$$L_h = 1 - i\frac{2}{k_n}(F + iG)$$

$$L_\alpha = \frac{1}{2} - i\frac{1}{k_n}\left[1 + 2(F + iG)\right] - 2\left(\frac{1}{k_n}\right)^2 (F + iG)$$

$$M_h = \frac{1}{2}$$

$$M_\alpha = \frac{3}{8} - i\frac{1}{k_n}$$

in which F and G are the aerodynamic functions derived in reference 6.

REFERENCES

1. Runyan, Harry L., and Sewall, John L.: Experimental Investigation of the Effects of Concentrated Weights on Flutter Characteristics of a Straight Cantilever Wing. NACA TN 1594, 1948.

2. Runyan, Harry L., and Watkins, Charles E.: Flutter of a Uniform Wing with an Arbitrarily Placed Mass According to a Differential-Equation Analysis and a Comparison with Experiment. NACA Rep. 966, 1950. (Formerly NACA TN 1848.)

3. Woolston, Donald S., and Runyan, Harry L.: Appraisal of Method of Flutter Analysis Based on Chosen Modes by Comparison with Experiment for Cases of Large Mass Coupling. NACA TN 1902, 1949.

4. Woolston, Donald S., and Runyan, Harry L.: On the Use of Coupled Modal Functions in Flutter Analysis. NACA TN 2375, 1951.

5. Barmby, J. G., Cunningham, H. J., and Garrick, I. E.: Study of Effects of Sweep on the Flutter of Cantilever Wings. NACA TN 2121, 1950.

6. Theodorsen, Theodore: General Theory of Aerodynamic Instability and the Mechanism of Flutter. NACA Rep. 496, 1935.

7. Smilg, Benjamin, and Wasserman, Lee S.: Application of Three-Dimensional Flutter Theory to Aircraft Structures. ACTR No. 4798, Materiel Div., Army Air Corps, July 9, 1942.

8. Benun, D., and Waterman, L. T.: Aerodynamic Coef. for Three Dim. Flutter Analysis. Rep. No. R-146, Curtiss-Wright Corp., Airplane Div. (St. Louis), June 6, 1944.

9. Houbolt, John C., and Anderson, Roger A.: Calculation of Uncoupled Modes and Frequencies in Bending or Torsion of Nonuniform Beams. NACA TN 1522, 1948.

10. Wasserman, Lee S., Mykytow, Walter J., and Spielberg, Irvin: Tab Flutter Theory and Application. AAF TR No. 5153, Air Technical Service Command, Army Air Forces, Sept. 1, 1944.

TABLE I

DISTRIBUTION OF GEOMETRIC AND INERTIAL PROPERTIES

OF NONUNIFORM SWEPTBACK CONFIGURATION

Wing segment	η	b (ft)	x_α	a	r_α^2
1	0.0415	0.425	0.171	-0.308	0.245
2	.124	.404	.167	-.301	.250
3	.207	.386	.140	-.292	.232
4	.298	.363	[a]-.350	-.274	[a].443
5	.373	.346	.157	-.260	.220
6	.456	.325	.090	-.244	.231
7	.539	.304	.082	-.236	.223
8	.622	.286	.090	-.222	.233
9	.705	.269	.118	-.263	.223
10	.796	.247	[a].164	-.272	[a].461
11	.871	.229	.091	-.237	.224
12	.953	.206	.121	-.223	.226

[a]Value given for this segment includes concentrated weight.

TABLE II

EXPERIMENTAL DATA AND PERTINENT TUNNEL CONDITIONS

Run	Root condition	V_e (fps)	ρ (slugs/cu ft)	V_i (fps)	Percentage of Freon-12	M	Frequencies				Coefficients of structural damping[a]			Reynolds number[b]
							f_1 (cps)	f_2 (cps)	f_3 (cps)	f_e (cps)	g_1	g_2	g_3	
1	With restraint	283.3	0.007059	488.0	88.0	0.534	6.97	30.9	37.9	20.1	0.021	Poor record	0.026	5.77×10^6
2	Without restraint	292.1	.006306	476.0	78.8	.534	6.28	26.1	36.6	18.0	.019	0.019	.017	5.19×10^6

[a] Numerical subscripts for these coefficients correspond to order of appearance of natural frequencies.

[b] These values are based on the mean aerodynamic chord (see fig. 1 for location).

TABLE III

SUMMARY OF THEORETICAL AND EXPERIMENTAL RESULTS

Run	Density (slugs/cu ft)	Modes employed in calculations	Theoretical		Experimental	
			v_Λ (fps)	f_Λ (cps)	v_e (fps)	f_e (cps)
1	0.007059	1st bending, 1st torsion	261.5	23.6	283.3	20.1
1	.007059	1st bending, 1st torsion, 2nd bending	255.0	23.0	283.3	20.1
1	.007059	1st bending, 1st torsion, 2nd torsion	260.0	23.5	283.3	20.1
1	.007059	1st bending, 1st torsion, 2nd bending, 2nd torsion	255.0	23.0	283.3	20.1
2[a]	.006306	1st bending, 1st torsion	275.5	23.4	292.1	18.0

[a]Data for run 2 were obtained without root restraint.

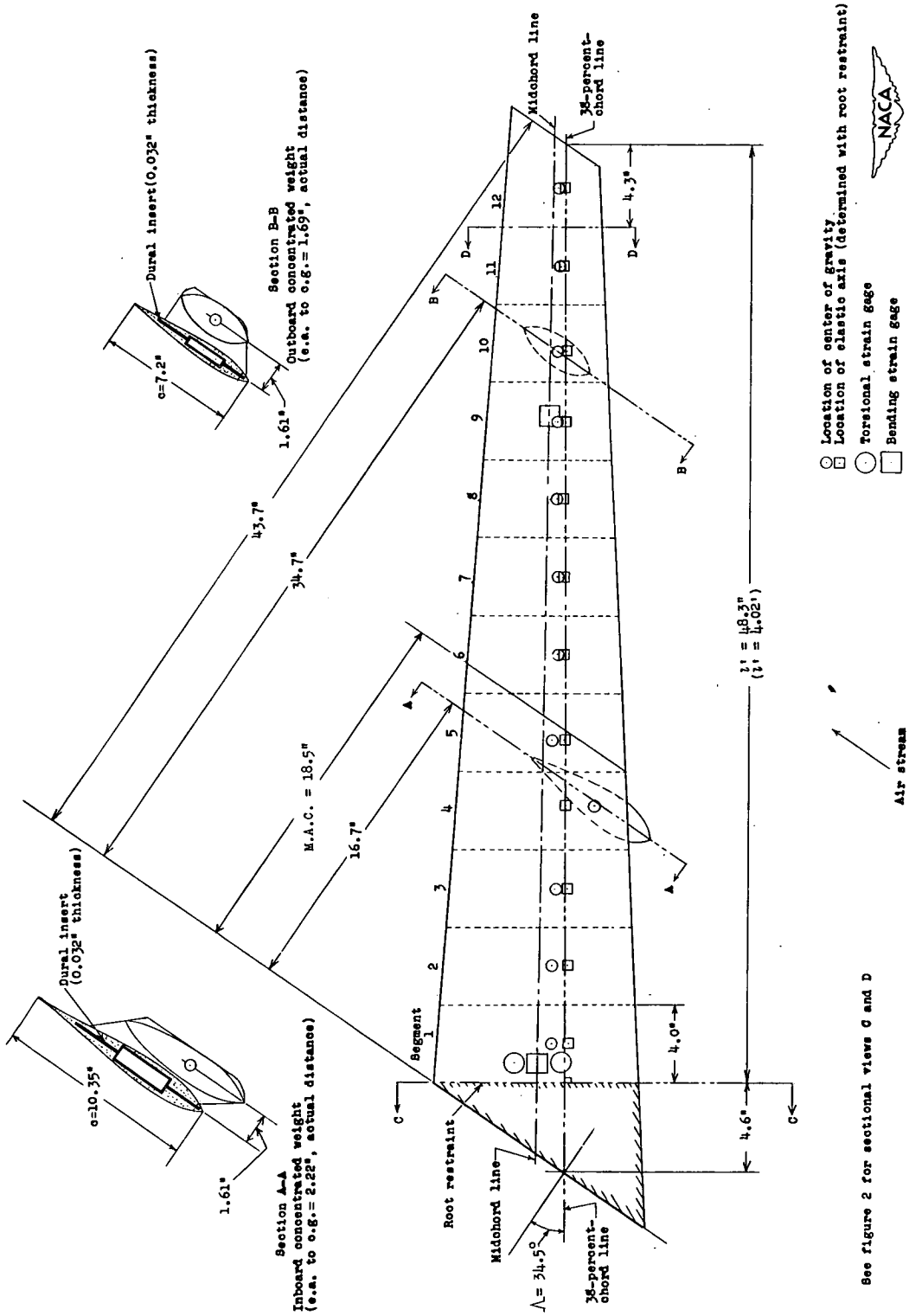

Figure 1.- Plan view of wing.

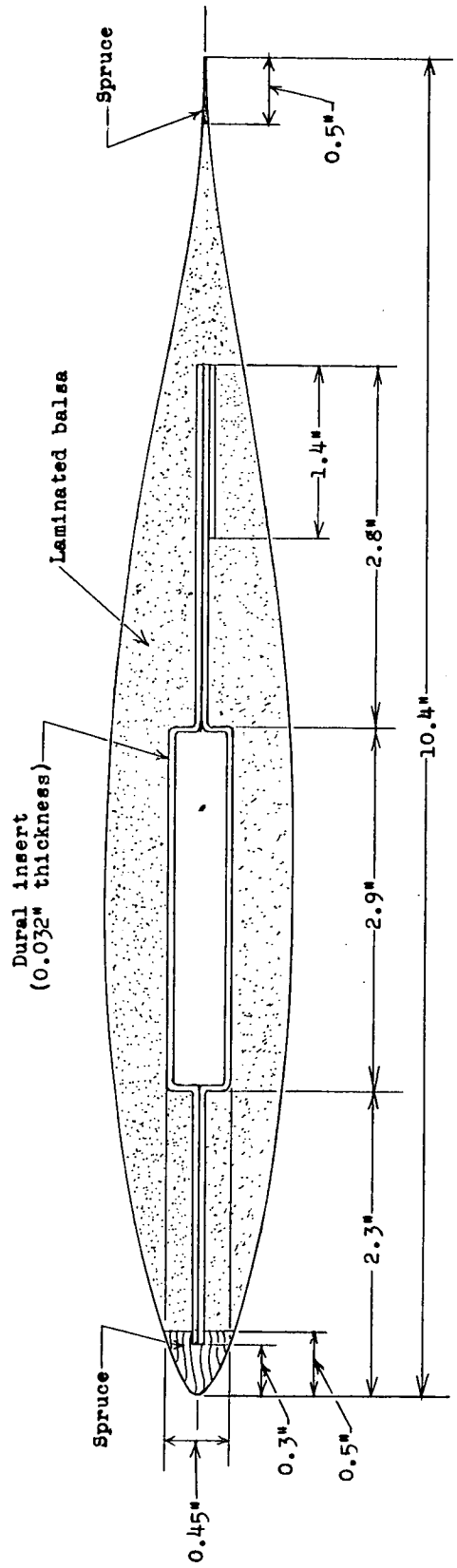

Section C-C(see figure 1)

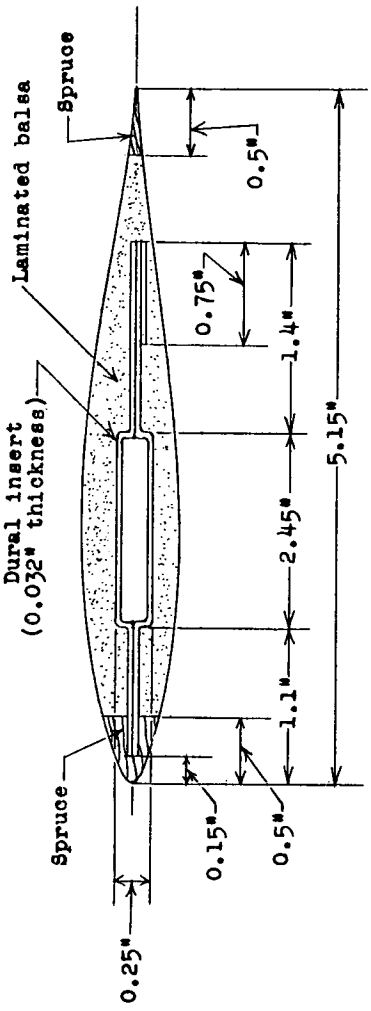

Section D-D(see figure 1)

Figure 2.- Cross-sectional views of model.

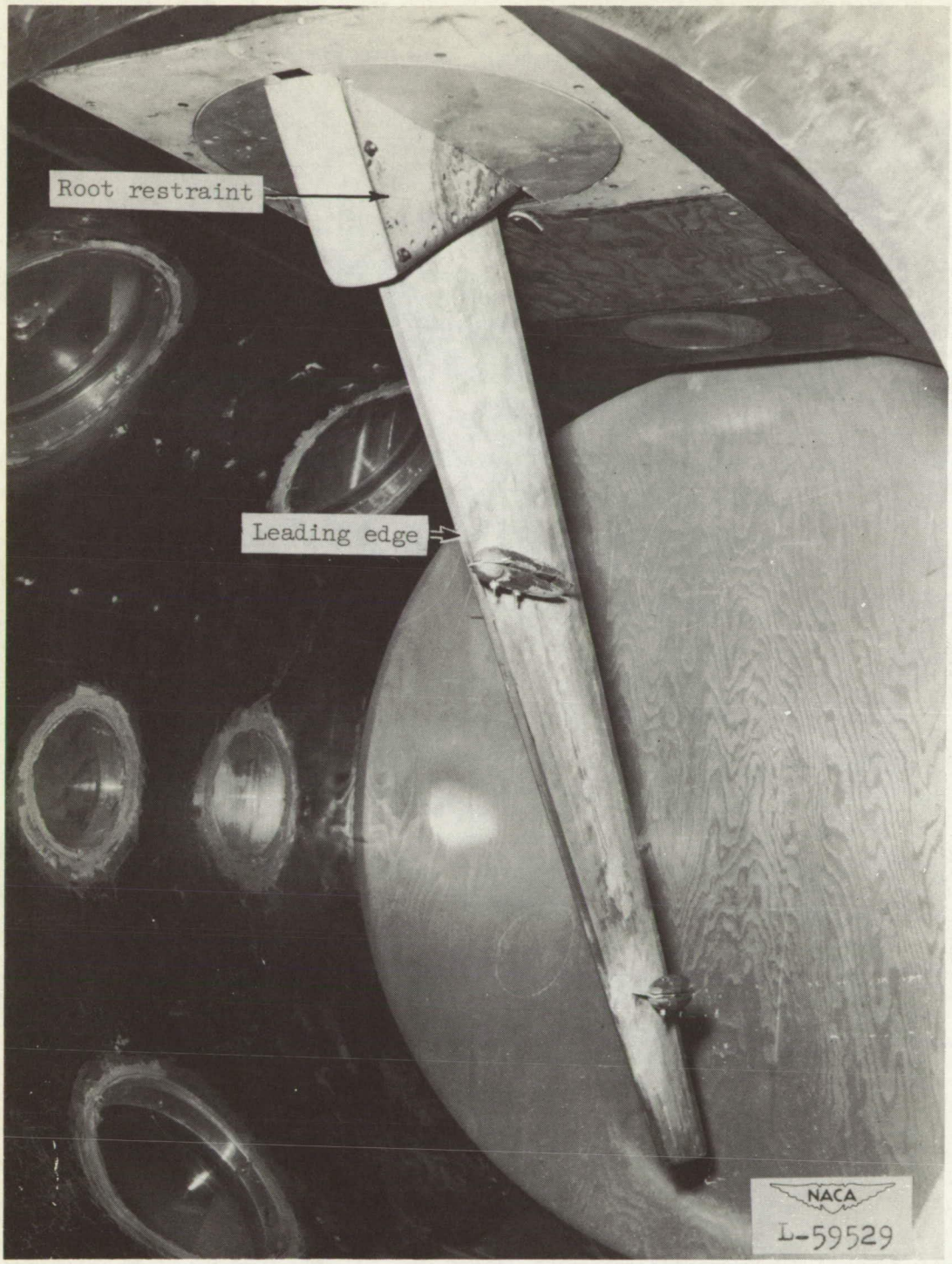

Figure 3.- General view of test section showing wing with concentrated weights and root restraint.

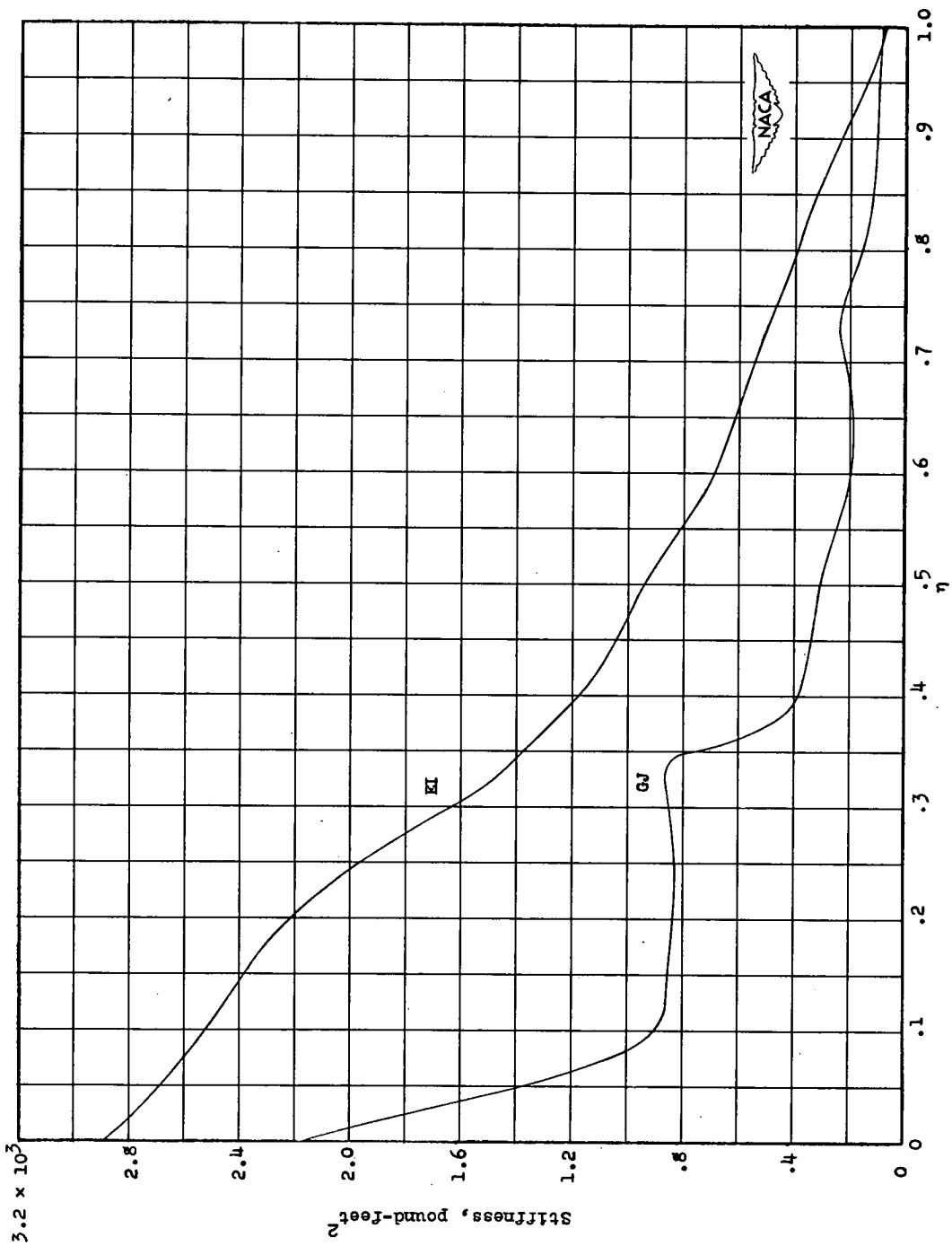

Figure 4.- Lengthwise distribution of bending and torsional stiffnesses of wing.

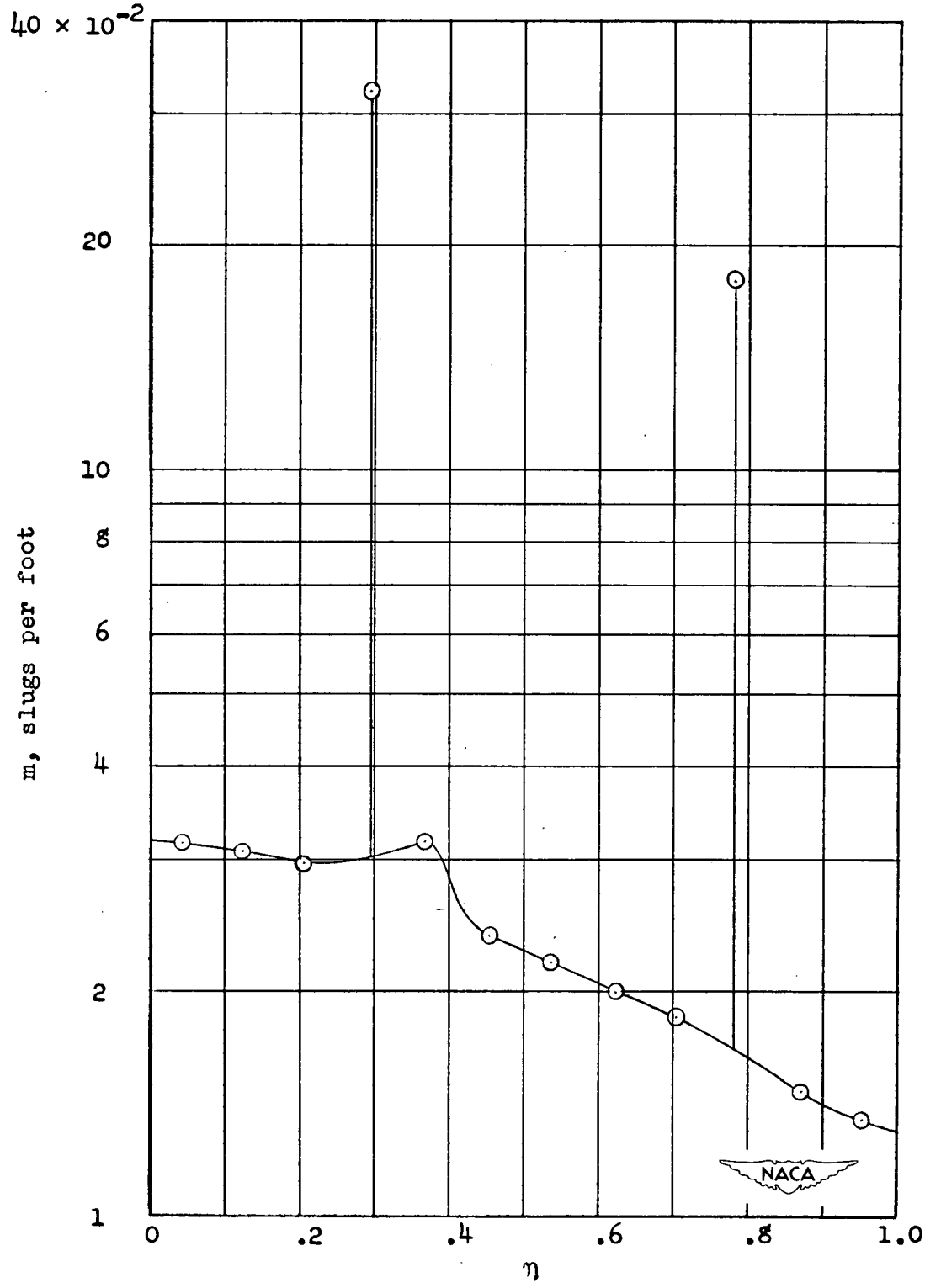

Figure 5.- Lengthwise distribution of mass (per unit length) of wing and concentrated weights.

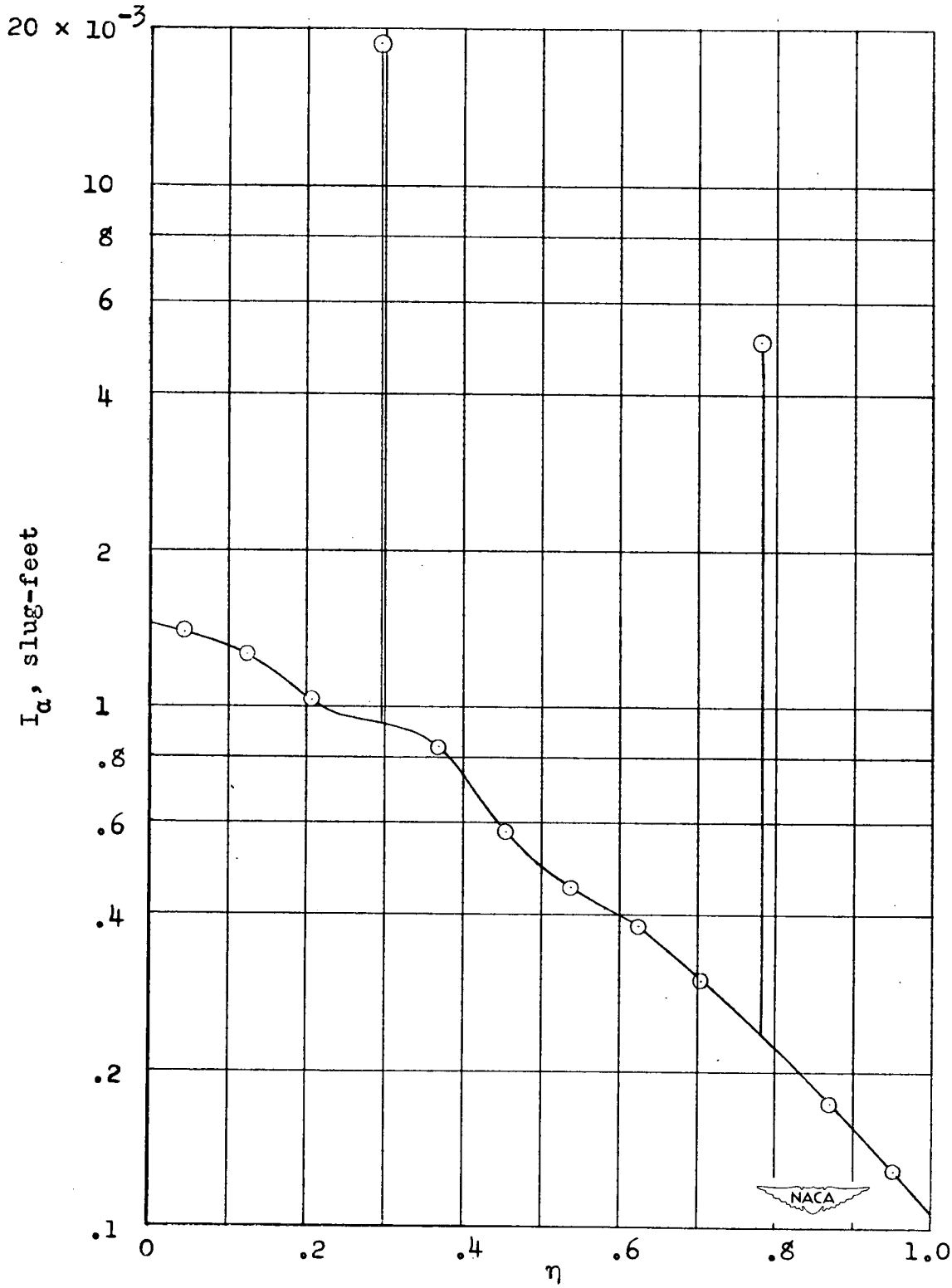

Figure 6.- Lengthwise distribution of mass moment of inertia (per unit length) of wing and concentrated weights.

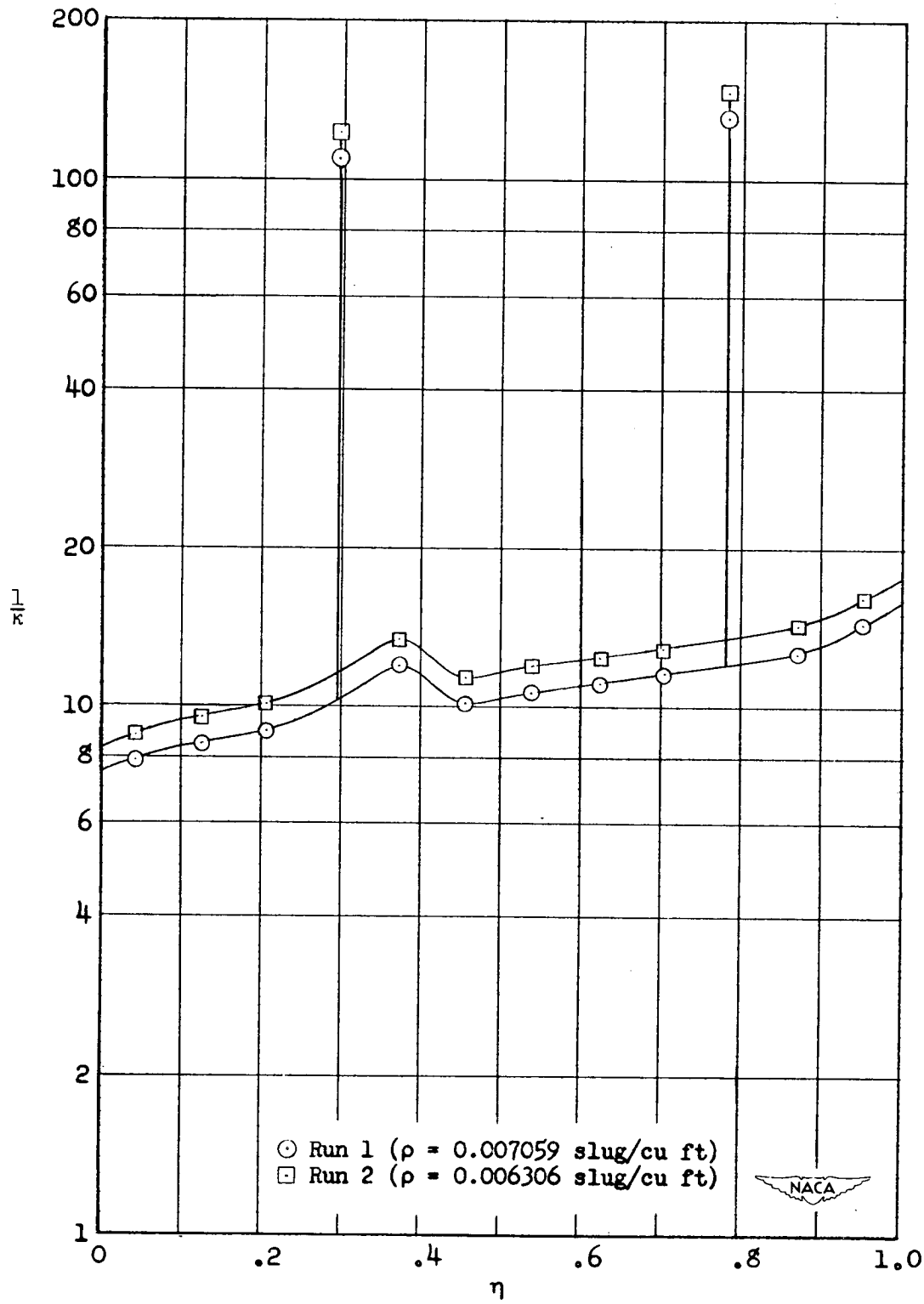

Figure 7.- Lengthwise distribution of mass-density ratio for both flutter runs.

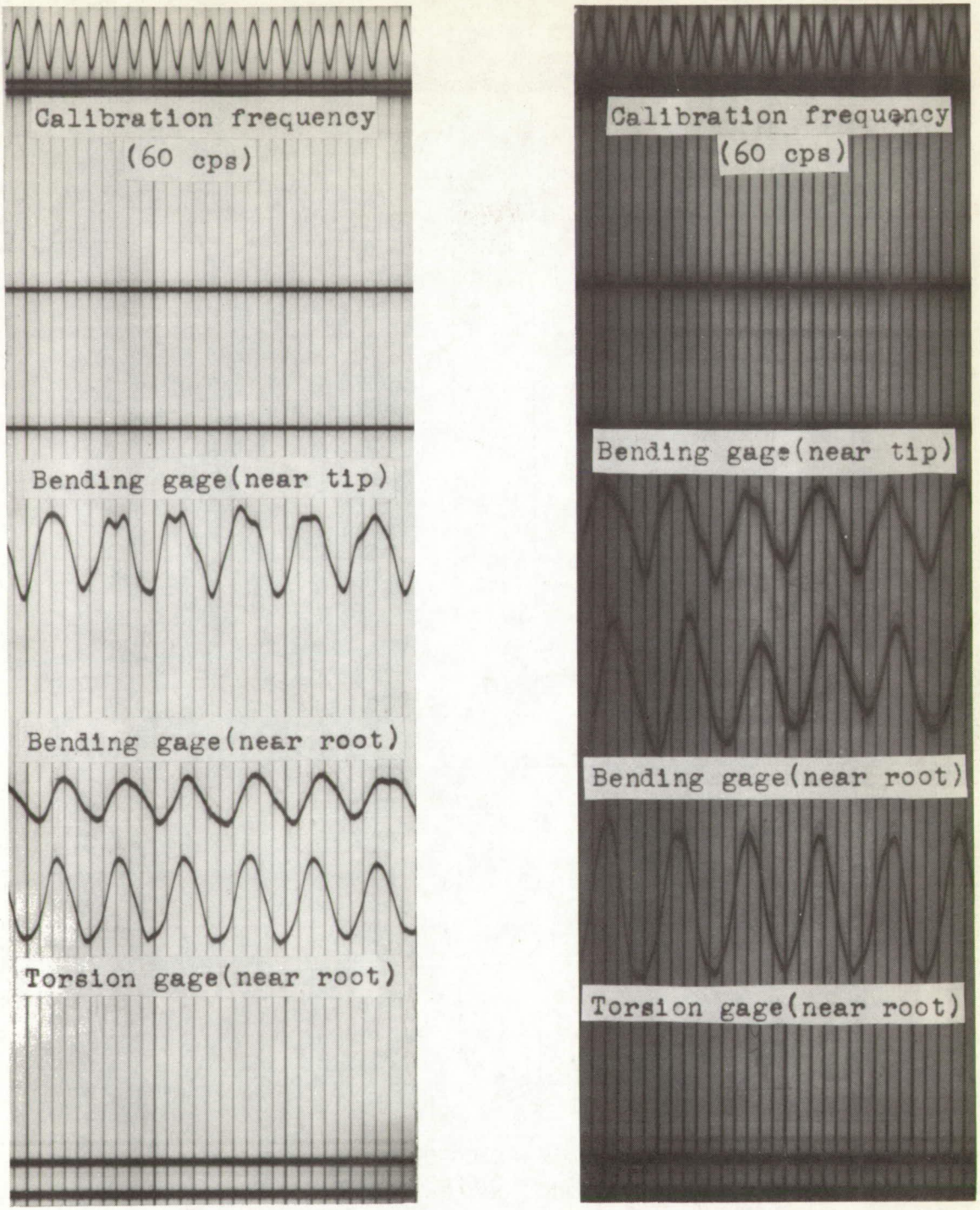

(a) Run 1. (b) Run 2.

Figure 8.- Oscillograph records during flutter of wing-weight configuration.

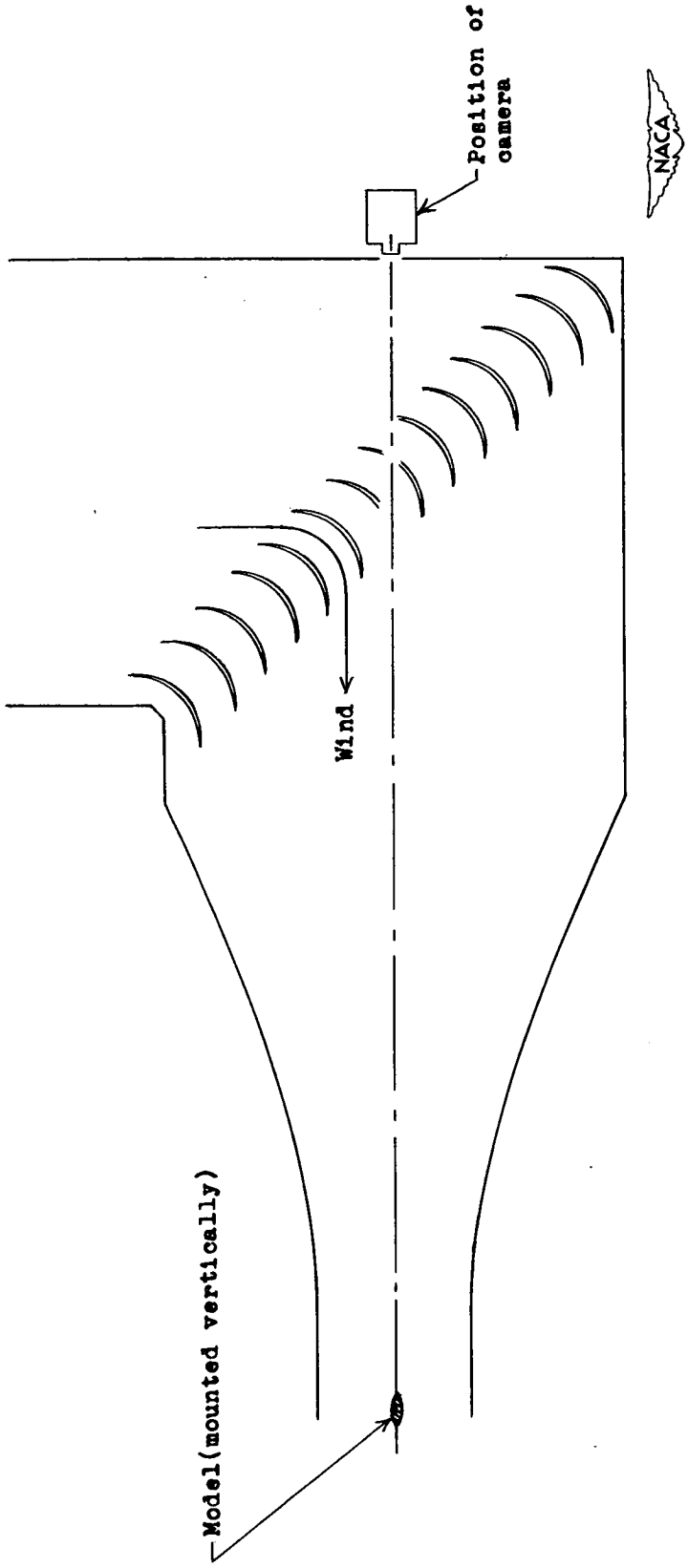

Figure 9.- Plan view of entrance cone and test section of Langley 4.5-foot flutter research tunnel showing the location of the motion-picture camera in relation to the test section.

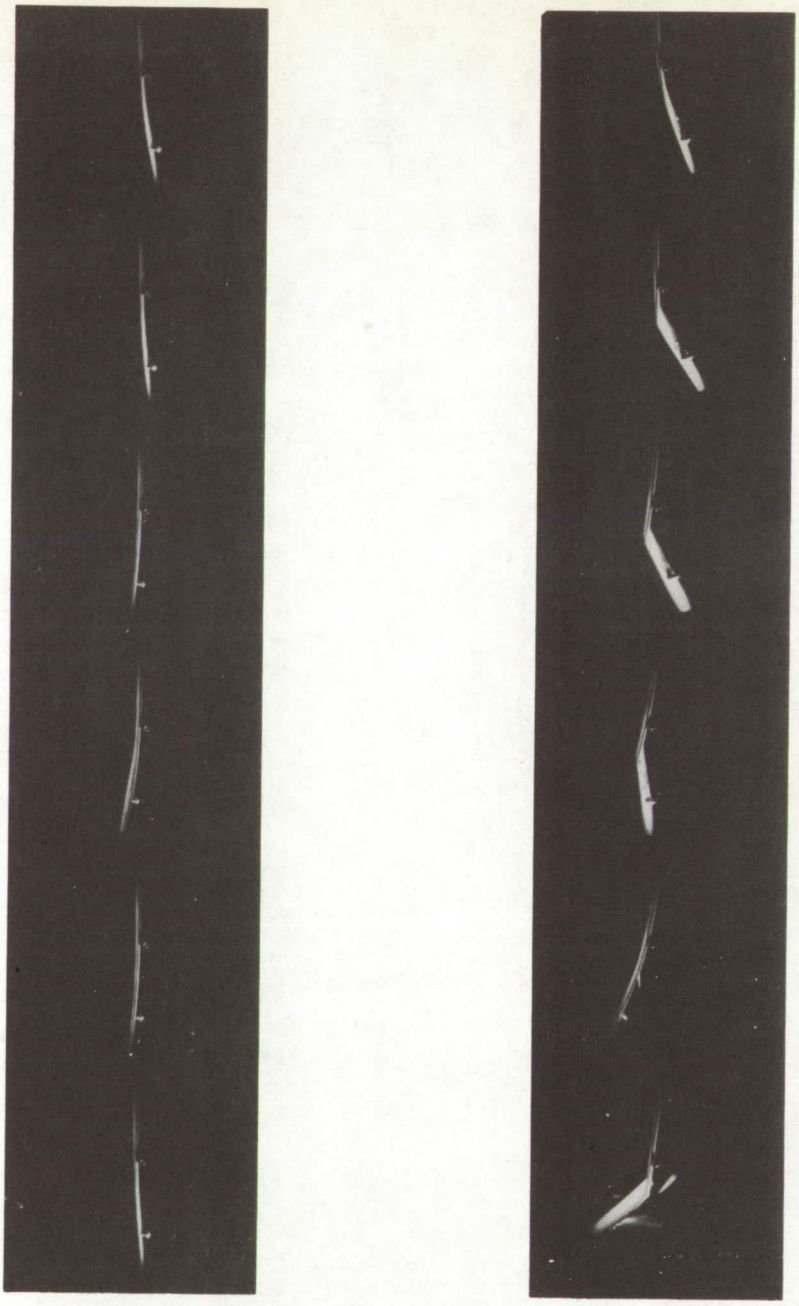

(a) Run 2 (without root restraint).

(b) Run on similar model which fluttered to destruction.

NACA
L-70775

Figure 10.- High-speed motion-pictures showing 1 cycle of flutter for each of two similar sweptback wings carrying two concentrated weights. The direction of increasing time is from top to bottom, and the cantilevered or fixed end of the wing is at the top of each picture.

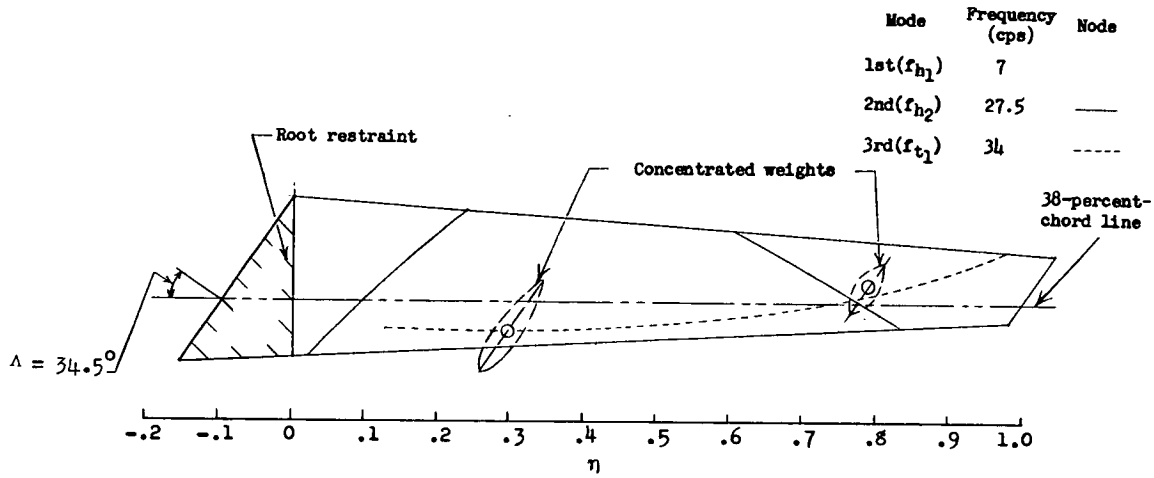

(a) With root restraint.

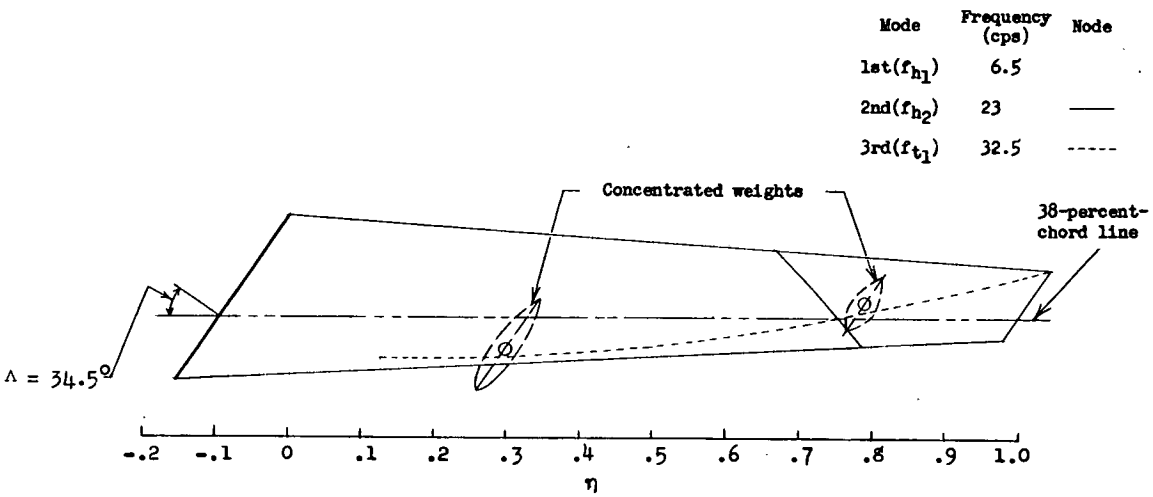

(b) Without root restraint.

Figure 11.- Nodal patterns and corresponding natural frequencies for wing-weight configuration nearly the same as that used in analytical investigation.

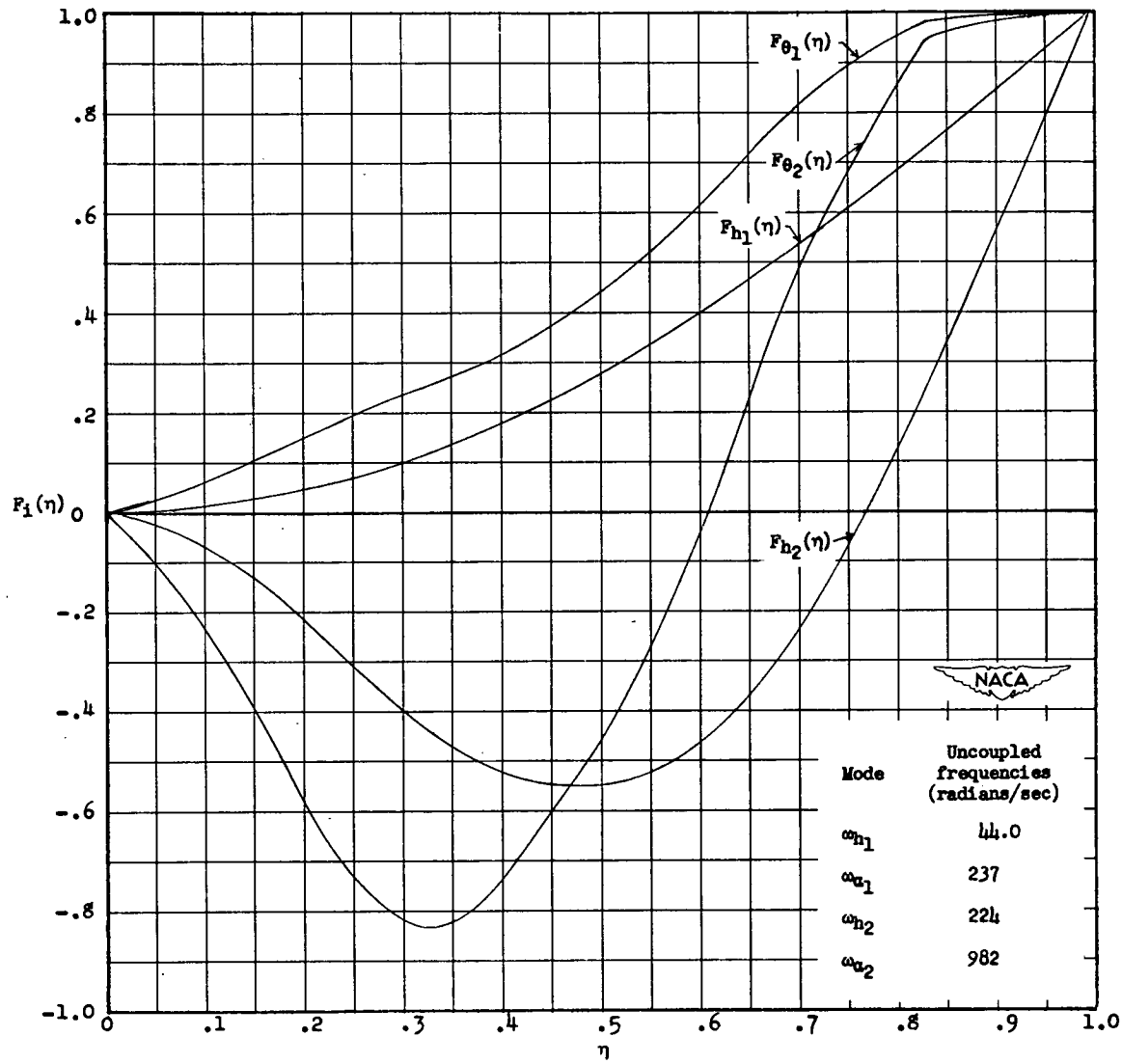

Figure 12.- Uncoupled bending and torsion modes and frequencies for nonuniform sweptback cantilever wing with two concentrated weights.

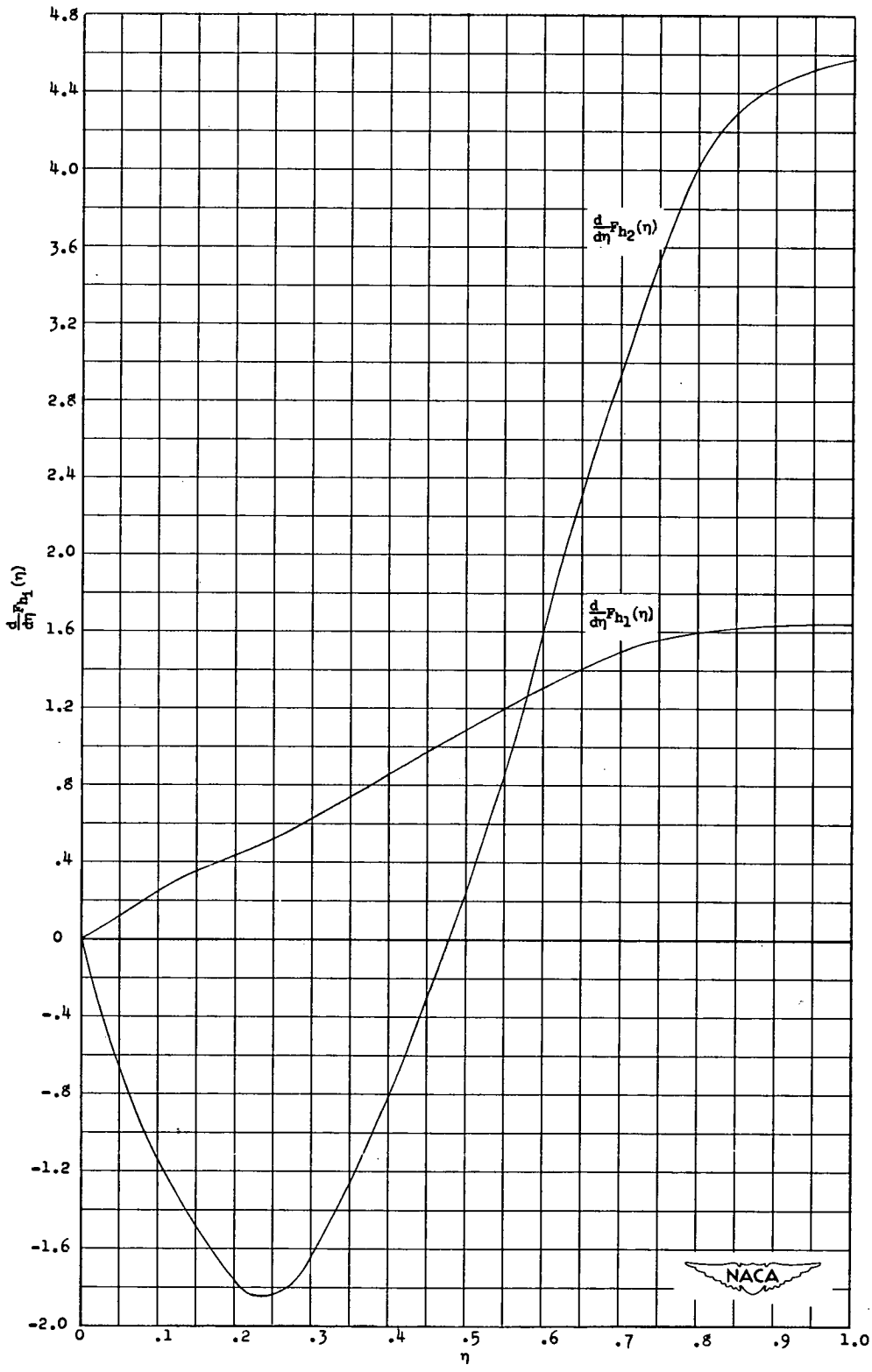

Figure 13.- Slopes of uncoupled bending modes shown in figure 12.